Interrelationships among Snow Distribution, Snowmelt, and Snow Cover Depletion: Implications for Atmospheric, Hydrologic, and Ecologic Modeling

GLEN E. LISTON

Department of Atmospheric Science, Colorado State University, Fort Collins, Colorado

(Manuscript received 5 October 1998, in final form 21 December 1998)

ABSTRACT

Local, regional, and global atmospheric, hydrologic, and ecologic models used to simulate weather, climate, land surface moisture, and vegetation processes all commonly represent their computational domains by a collection of finite areas or grid cells. Within each of these cells three fundamental features are required to describe the evolution of seasonal snow cover from the end of winter through spring melt. These three features are 1) the within-grid snow water equivalent (SWE) distribution, 2) the gridcell melt rate, and 3) the within-grid depletion of snow-covered area. This paper defines the exact mathematical interrelationships among these three features and demonstrates how knowledge of any two of them allows generation of the third. During snowmelt, the spatially variable subgrid SWE depth distribution is largely responsible for the patchy mosaic of snow and vegetation that develops as the snow melts. Applying the melt rate to the within-grid snow distribution leads to the exposure of vegetation, and the subgrid-scale vegetation exposure influences the snowmelt rate and the grid-averaged surface fluxes. By using the developed interrelationships, the fundamental subgrid-scale features of the seasonal snow cover evolution and the associated energy and moisture fluxes can be simulated using a combination of remote sensing products that define the snow-covered area evolution and a submodel that appropriately handles the snowmelt computation. Alternatively, knowledge of the subgrid SWE distribution can be used as a substitute for the snow-covered area information.

1. Introduction

With its high albedo, low thermal conductivity, and considerable spatial and temporal variability, seasonal snow cover overlying land plays a key role in governing the earth's global radiation balance; this balance is the primary driver of the earth's atmospheric circulation system and associated climate. Of the various features that influence the surface radiation balance, the location and duration of snow cover compose two of the most important seasonal variables. In the Northern Hemisphere the mean monthly land area covered by snow ranges from 7% to 40% during the annual cycle, making snow cover the most rapidly varying large-scale surface feature on the earth (Hall 1988).

The problem of realistically representing seasonal snow in regional and global atmospheric and hydrologic models is made complex because of the numerous snow-related features that display considerable spatial variability at scales below those resolved by the models. As an example of this variability, over the winter landscape in middle and high latitudes the interactions among wind, vegetation, topography, precipitation, solar radiation, and snowfall produce snow covers of nonuniform depth and density (e.g., Liston and Sturm 1998). During the melt of these snow covers, the snow-depth variation leads to a patchy mosaic of vegetation and snow cover that evolves as the snow melts (e.g., Shook et al. 1993). This mix of snow and vegetation strongly influences the energy fluxes returned to the atmosphere and the associated feedbacks that accelerate the melting of remaining snow-covered areas. From the perspective of a surface energy balance, the interactions between the land and atmosphere are particularly complex during this melt period (Liston 1995; Essery 1997; Neumann and Marsh 1998). The variable snow distribution also can play an important role in determining the timing and magnitude of snowmelt runoff, and the end-of-winter snow distribution is a crucial input to snowmelt hydrology models, including those used for water resource management (e.g., U.S. Army Corps of Engineers 1956; Male and Gray 1981; Martinec and Rango 1986; WMO 1986; Kane et al. 1991). In Arctic tundra and alpine regions the uneven distribution of snow exerts strong control over plant community distribution (Evans et al. 1989; Walker et al. 1993), and in the forest–alpine ecotone the snow distribution influences tree distributions and growth characteristics (Griggs 1938; Billings 1969; Daly 1984; Wooldridge et al. 1996).

Corresponding author address: Dr. Glen E. Liston, Dept. of Atmospheric Science, Colorado State University, Fort Collins, CO 80523. E-mail: liston@iceberg.atmos.colostate.edu

In light of the role that snow plays in influencing land and atmospheric processes, it is essential that local, regional, and global models used to simulate weather, climate, hydrologic, and ecologic interactions be capable of accurately describing the seasonal snow evolution. In recent years, significant strides have been made to represent snow cover better in climate models (Verseghy 1991; Lynch-Stieglitz 1994; Marshall and Oglesby 1994; Marshall et al. 1994; Douville et al. 1995; Yang et al. 1997; Loth and Graf 1998a; Slater et al. 1998), but there are still studies that indicate that current climate model simulations of seasonal snow do not reproduce the observed snow distributions (e.g., Foster et al. 1996). Typically, snow accumulation and melt in climate models are simulated by applying simple energy and mass balance accounting procedures (Foster et al. 1996). These algorithms frequently neglect or oversimplify important physical processes such as those associated with subgrid-scale temporal and spatial variability of snow-covered area. The lack of subgrid snow distribution representations in most climate models has been acknowledged as a deficiency in snow cover evolution and atmospheric interaction simulations (Loth and Graf 1998b). Walland and Simmonds (1996) introduced one method to address this deficiency. To account for snow distribution–related processes in weather, climate, hydrologic, and ecologic models, accurate descriptions of grid-scale and subgrid-scale snow distributions are necessary.

At its most basic foundation, capturing the fundamental aspects of snow cover evolution within a model grid cell requires addressing three primary features. Conceptually, these three relate directly to

1) the snow cover has some spatial distribution (for example, over a parking lot or a relatively flat prairie landscape the distribution generally is uniform, while in windblown and topographically variable regions the distribution can be quite nonuniform),
2) at some point during the year the snow cover experiences melting, and
3) eventually, as part of the snowmelt process, the snow cover disappears and exposes the underlying surface (usually soil and low-growing vegetation).

While at first glance these three features may appear overly simplistic, they are coupled so strongly that any unrealistic model gridcell description of one of them leads to the misrepresentation of the others. This misrepresentation, in turn, has important consequences for model-computed energy and moisture fluxes.

Through a combination of meteorological observations, spatially distributed snow water equivalent (SWE) depth measurements, and snow cover depletion observations, Liston (1986) suggested that there must be a strong interrelationship among snowmelt, snow distribution, and snow cover depletion. Cline et al. (1998) discussed and applied a ''conceptual'' snow cover depletion model in which the premelt SWE depth is a function of snow cover duration and accumulated melt energy at a particular site, and similar relationships have been used implicitly as part of other, primarily hydrologic, studies (e.g., Dunne and Leopold 1978; Rango and Martinec 1979; Martinec and Rango 1981, 1987; Ferguson 1984; Buttle and McDonnell 1987; Rango 1993; Cline 1997; König and Sturm 1998). While these studies have, in some way, made use of the relationships among snow cover melt, distribution, and areal depletion, the exact mathematical interrelationships that form the basis of these studies have never been defined, and a more explicit and complete discussion of these features is warranted. This paper provides a mathematical description of the general conceptual model that has been used in the past and lays the foundation for the next generation of models that will include improved realism in their snow distribution representations. This mathematical description will formalize the general assumptions adopted in the hydrologic studies cited above and will provide a sound theoretical framework for implementing these ideas in atmospheric and ecologic models. In addition, it will provide valuable insight into how these interrelationships can be used to improve seasonal snow cover simulations. Specifically, the mathematical interrelationships among snow cover melt, snow distribution, and snow cover areal depletion within a model grid cell will be presented and discussed within the context of atmospheric, hydrologic, and ecologic modeling efforts.

2. Mathematical formulation

Initially, for the purpose of the following presentation, the natural system that will be discussed will follow the snow evolution pattern observed in much of the Arctic, where the seasons are well defined; winter is largely a period of snow accumulation and no melting, and spring is largely a period of melting and no snow accumulation. Thus, winter leads to an end-of-winter snow distribution and is followed by a spring melt period that proceeds until the snow is gone. In middle latitudes, the snow cover generally undergoes numerous such ''winter–spring'' events during the course of a year; the relaxation of this simplified ''arctic'' behavior will be discussed later in this paper. In addition, it is understood that from the perspective of the atmosphere and large-feature hydrologic system the first-order effect is whether there is snow on the ground; this importance arises primarily because of the large albedo differences between snow and other (nonice) surfaces and the maximum 0°C snow surface temperature constraint (e.g., Liston 1995). These two factors dominate the gridcell surface energy balance to the extent that it is not possible, without significantly misrepresenting the governing physics, to simulate the correct moisture and energy fluxes unless the gridcell snow-covered fraction is known. To simplify the discussion it also is assumed that the bulk, or vertically integrated, average snow density is known; thus, the terms ''snow depth'' and ''SWE

depth'' will be used interchangeably, with the understanding that the snow depths always can be converted to an SWE depth by applying the snow (and water) density. The term ''melt rate'' refers to moisture lost from the snow cover, and the ''exposure of vegetation'' refers to exposing the surface that was previously covered by snow. This surface can be any type, including the low-stature rock, low-growing vegetation, and bare ground found on the prairies and in Arctic and alpine regions, or it can be the surfaces found under deciduous and evergreen forest canopies.

Under the simple Arctic-type winter–spring snow history, for each model grid cell three fundamental features are required to describe the evolution of snow cover from the end of winter through spring melt. These three fundamental features are

1) the end-of-winter (premelt) SWE distribution,
2) the melt rate, and
3) the depletion of snow-covered area.

Throughout this paper, an Arctic Alaska example in which snow distribution and atmospheric-forcing data are known will be used to help to illustrate the interrelationships among these three features. This example can be considered to represent an atmospheric, hydrologic, or ecologic model grid cell. Figure 1 (6 May panel) describes the example snow distribution taken from Imnavait Creek, Alaska (Liston and Sturm 1998). This area is located between the headwaters of the Kuparuk and Toolik Rivers at 68°37′N, 149°17′W and an elevation of approximately 900 m. The vegetation covering the site is composed of low-growing sedges and grasses roughly 15 cm in height and occasional groupings of taller willows approximately 40 cm high, located in hillside water tracts and valley bottoms. Tussock tundra covers much of the area, with swampy features in the valley bottoms and dry rocky outcroppings on the exposed ridges. The topography is characterized by gently rolling ridges and valleys that have wavelengths of 1–2 km and amplitudes of 25–75 m (Fig. 1). Also within the domain are several more-pronounced topographic features that have much shorter and steeper slopes (up to 30° slopes over distances of a few tens of meters). The prevailing winds in Fig. 1 are from the southwest and lead to erosion on south- and west-facing slopes and increased snow accumulations on north- and east-facing slopes. Figure 2 summarizes the example hourly meteorological forcing, assumed to be representative over the domain of Fig. 1. These meteorological observations were collected from a tower located at approximately 2 km north and 1.2 km east in the Fig. 1 domain and were provided by the Water Research Center, University of Alaska, Fairbanks.

The three fundamental features required to describe the snow cover evolution can be generated from Figs. 1 and 2. The atmospheric forcing data of Fig. 2 are used to compute the snowmelt rate (Fig. 3a) by applying the surface energy balance model

$$(1 - \alpha)Q_{si} + Q_{li} + Q_{le} + Q_h + Q_e + Q_c = Q_m, \quad (1)$$

where Q_{si} is the solar radiation reaching the surface of the earth, Q_{li} is the incoming longwave radiation, Q_{le} is the emitted longwave radiation, Q_h is the turbulent exchange of sensible heat, Q_e is the turbulent exchange of latent heat, Q_c is the conductive energy transport, Q_m is the energy flux available for melt, and α is the surface albedo. Details of the formulation of each term in Eq. (1) and the model solution can be found in Liston (1995), Liston and Hall (1995), and Liston et al. (1999b). In this model, each term in the surface energy balance is computed by applying general equations that have been cast in a form that leaves the surface temperature as the only unknown. The melt energy is defined to be zero, and Eq. (1) is solved iteratively for the surface temperature. In the presence of snow, resultant surface temperatures greater than 0°C indicate that energy is available for melting. The amount of available melt energy then is computed by fixing the surface temperature at 0°C and solving Eq. (1) for Q_m. Under melting conditions, the snow surface is considered to be fully saturated and vertically isothermal. For the purposes of the current discussion, this melt rate equals the moisture lost from the snow cover (although it is recognized that in the natural system there may be delays between melt and snow cover moisture loss caused by such processes as percolation and refreezing). The end-of-winter snow distribution of Fig. 1 (6 May panel) is presented as a histogram in Fig. 3b, and applying the daily melt rates from Fig. 3a to the distribution of Fig. 1 yields the snow cover depletion in Fig. 3c. Implicit in this approach is that the melt rates of Fig. 3a are applicable to the entire domain given in Fig. 1 and represented by Figs. 3b and 3c.

Figures 3a–c are interrelated strongly and knowledge of any two of them allows the generation of the third. When the melt rates of Fig. 3a are applied to the snow distribution of Fig. 3b, the snow-covered area is depleted according to the curve in Fig. 3c. It is not so obvious that the melt rates (Fig. 3a) can be derived from the snow cover depletion (Fig. 3c) and the snow distribution (Fig. 3b). Last, and maybe even more important, is that the snow distribution (Fig. 3b) can be derived from the melt rates (Fig. 3a) and the snow cover depletion (Fig. 3c). This last point has major implications for regional- and global-scale atmospheric and hydrologic modeling because melt rates can be computed from readily available atmospheric quantities (such as those collected as part of local and worldwide observational networks and those generated at atmospheric analysis and forecast centers), and the snow cover depletion curves are becoming readily available as part of National Aeronautics and Space Administration (NASA) (Hall et al. 1995) and National Operational Hydrologic Remote Sensing Center (NOHRSC) (http://www.nohrsc.nws.gov/) (Carroll 1997) snow cover remote sensing programs.

The exposure of vegetation (or loss of snow cover)

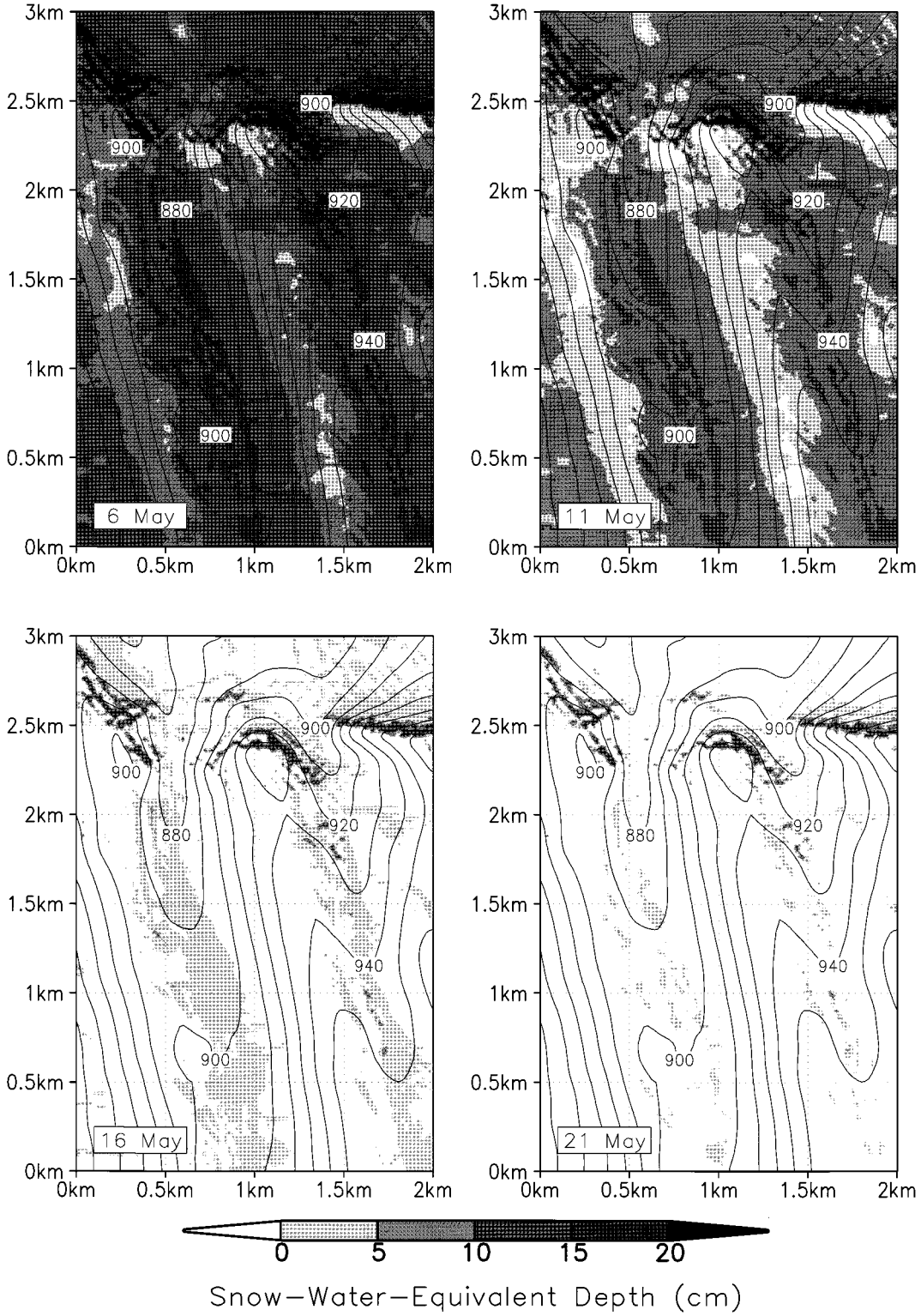

FIG. 1. End-of-winter (6 May panel) SWE distribution (gray shades) for Imnavait Creek, Arctic Alaska (Liston and Sturm 1998). Other panels show the distribution every five days during the melt period. Solid lines are topographic contours plotted using a 10-m contour interval.

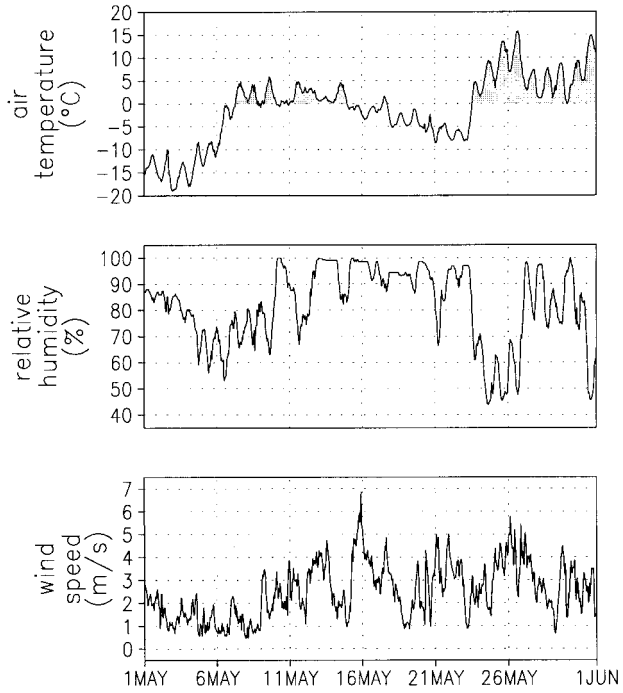

FIG. 2. Observed meteorological forcing used to compute melt rates for the Imnavait Creek domain given in Fig. 1. (Data courtesy of the Water Research Center, University of Alaska, Fairbanks.)

is related directly to the melt rate M_{rate} and SWE depth ζ. This relation is because, at a point (or over a uniform snow cover), the accumulated snowmelt M_{acc} at the time the vegetation is completely exposed is equal to the end-of-winter SWE depth. If this time t of snow cover disappearance is defined to be t^*, then the end-of-winter SWE depth (at that point) $\zeta_{\max}$ is

$$\zeta_{\max} = M_{\text{acc}}(t = t^*). \tag{2}$$

In addition, the accumulated melt is related to M_{rate} through

$$M_{\text{acc}}(t = t^*) = \int_{t=0}^{t=t^*} M_{\text{rate}}(t)\, dt. \tag{3}$$

As an example, applying the melt rate from Fig. 3a to Eq. (3) yields the melt-accumulation curve given in Fig. 4.

For a two-dimensional domain such as that in Fig. 1, which has a nonuniform end-of-winter SWE depth distribution (Fig. 1, 6 May panel), the same principle applies, but in this case, vegetation at each point within the domain is exposed at different times. Thus, at each point, the end-of-winter snow depth must equal the snowmelt accumulated up to the time at which that point became snow free. To illustrate the interrelationships for a spatial domain, some important concepts first must be defined. These defined concepts will be followed by a presentation of how they interrelate.

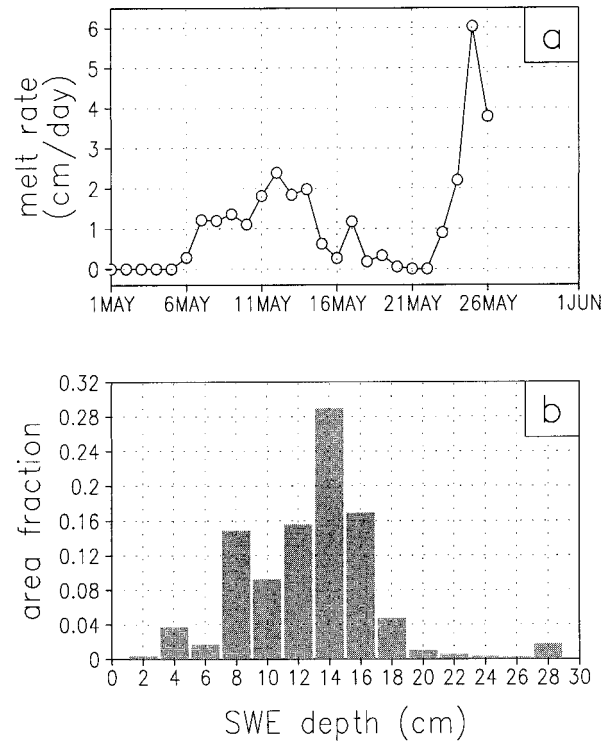

FIG. 3. (a) Melt rates computed from an energy balance model and observed meteorological forcing. (b) End-of-winter SWE distribution histogram computed from Fig. 1 (6 May panel). (c) Depletion of snow-covered area during the melt period for the domain of Fig. 1.

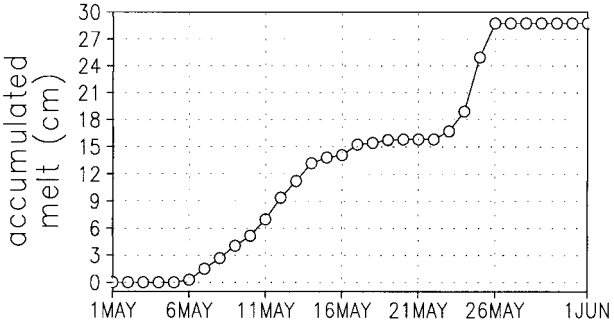

FIG. 4. Accumulated SWE depth of melt, from Fig. 3a.

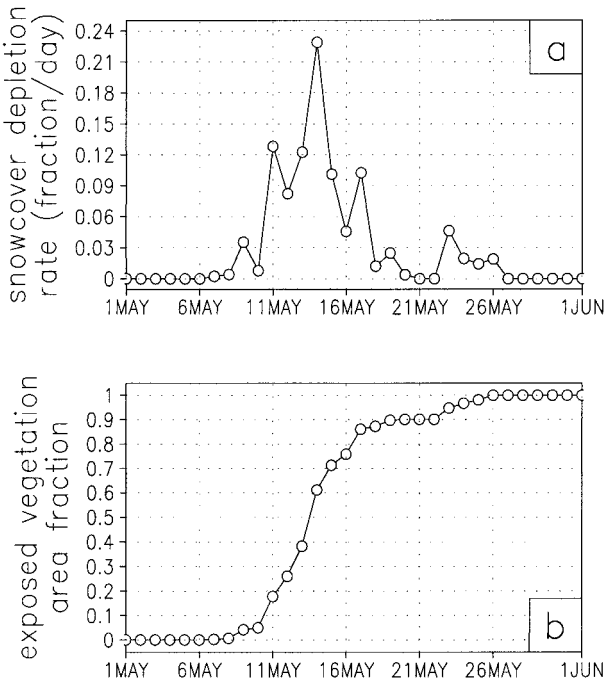

FIG. 5. (a) Snow cover depletion rate during the melt period, from Fig. 3c. (b) Exposure of vegetation during the melt period, from Fig. 3c.

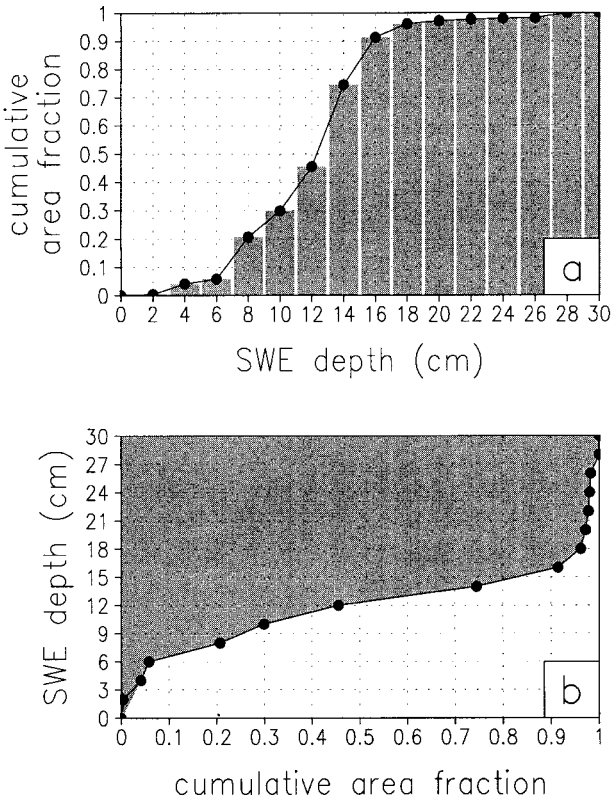

FIG. 6. (a) Integrated area-fraction end-of-winter SWE distribution for the domain of Fig. 1, from Fig. 3b. (b) The same information presented in (a) but with the axes exchanged.

The snow cover reduction rate (or vegetation exposure rate) S_{rate} is

$$S_{\text{rate}}(t) = -dS_{\text{frac}}(t)/dt, \tag{4}$$

where, using the Figs. 3a–c example, the snow-covered area fraction S_{frac} from Fig. 3c is used to compute the snow cover reduction rate in Fig. 5a. Integrating this snow cover reduction rate gives the exposed-vegetation area fraction V_{frac} for the domain at any time t^*,

$$V_{\text{frac}}(t = t^*) = \int_{t=0}^{t=t^*} S_{\text{rate}}(t)\, dt, \tag{5}$$

where, for the Figs. 3a–c example, the evolution is given in Fig. 5b. This vegetation fraction also is equal to

$$V_{\text{frac}}(t = t^*) = 1 - S_{\text{frac}}(t = t^*). \tag{6}$$

The fractional area A^* covered by SWE of some depth or less ζ_{max} is given by

$$A^*(0 \le \zeta \le \zeta_{\text{max}}) = \int_{\zeta=0}^{\zeta=\zeta_{\text{max}}} A(\zeta)\, d\zeta, \tag{7}$$

where, for the example, this distribution is given in Fig. 6a. This same snow distribution information can be presented in another way; in this case, ζ_{max} covering A^* is given by

$$\zeta_{\text{max}} = \int_{A=0}^{A=A^*} \zeta(A)\, dA, \tag{8}$$

where, for the example, this distribution is given in Fig. 6b.

From the identity given by Eq. (2), and

$$V_{\text{frac}}(t = t^*) = A^*(0 \le \zeta \le \zeta_{\text{max}}), \tag{9}$$

it follows from Eqs. (3) and (8), and Eqs. (5) and (7), that

$$\int_{t=0}^{t=t^*} M_{\text{rate}}(t)\, dt = \int_{A=0}^{A=A^*} \zeta(A)\, dA, \tag{10}$$

and

$$\int_{t=0}^{t=t^*} S_{\text{rate}}(t)\, dt = \int_{\zeta=0}^{\zeta=\zeta_{\text{max}}} A(\zeta)\, d\zeta, \tag{11}$$

respectively.

From Eq. (10), we see that the information contained within Figs. 3a and 3b can be used to generate the information contained within Fig. 3c. This possibility is because, after supplying t^* and solving for A^*, this A^* also is equal to V_{frac} by Eq. (9). Similarly, from Eq. (11), the information contained within Figs. 3b and 3c can be used to generate the information contained within Fig. 3a. This possibility is because, after supplying t^* and solving for ζ_{max}, this ζ_{max} also is equal to M_{rate} by Eq. (2).

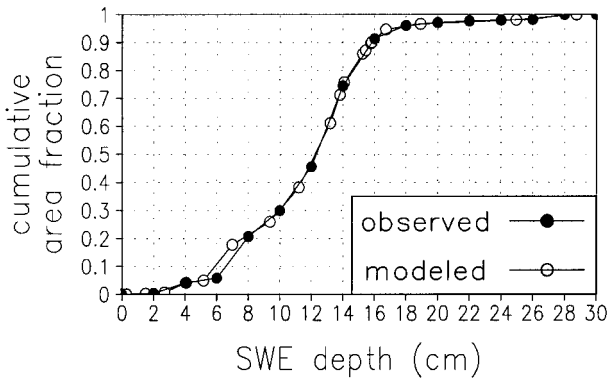

FIG. 7. Observed SWE distribution corresponding to that given in Fig. 6a, and the modeled distribution generated through a combination of Eqs. (12) and (13).

To generate the information contained within Fig. 3b from that in Figs. 3a and 3c, note that Eqs. (2) and (3), and Eqs. (5) and (9), suggest

$$\zeta_{\max} = \int_{t=0}^{t=t^*} M_{\text{rate}}(t)\, dt \tag{12}$$

and

$$A^*(0 \le \zeta \le \zeta_{\max}) = \int_{t=0}^{t=t^*} S_{\text{rate}}(t)\, dt, \tag{13}$$

respectively. Thus, inputs of any t^* that are common to both Eqs. (12) and (13) produce the $\zeta_{\max}$ and A^* values required to generate the snow distribution found in Fig. 3b. Applying this methodology to the example case yields the ''modeled'' snow distribution in Fig. 7; also included in Fig. 7 is the ''observed'' distribution corresponding to that given in Fig. 6a. In a more conceptual approach, the same Fig. 7 distribution can be generated by noting that Figs. 4 and 5b have a common x axis (time) and then plotting the area fraction against SWE depth for each common x (time) value. Last, the Fig. 3b distribution can be constructed by taking the derivative $dA^*/d\zeta_{\max}$ of the curve in Fig. 7.

Figures 3a–c, 4, 5, 6, and 7 have illustrated a numerical application of the preceding equations. A simple analytical example follows and will be used to highlight further application of the system of equations. For this example, let the melt rate be given by

$$M_{\text{rate}}(t) = \frac{t}{2} \qquad (0 \le t \le 10) \tag{14}$$

(Fig. 8a), and the time evolution of fractional snow cover be given by

$$S_{\text{frac}}(t) = 1 - \frac{t}{10} \qquad (0 \le t \le 10) \tag{15}$$

(Fig. 8b). Then, applying Eq. (15) to Eqs. (4) and Eq. (5), or Eq. (6), yields

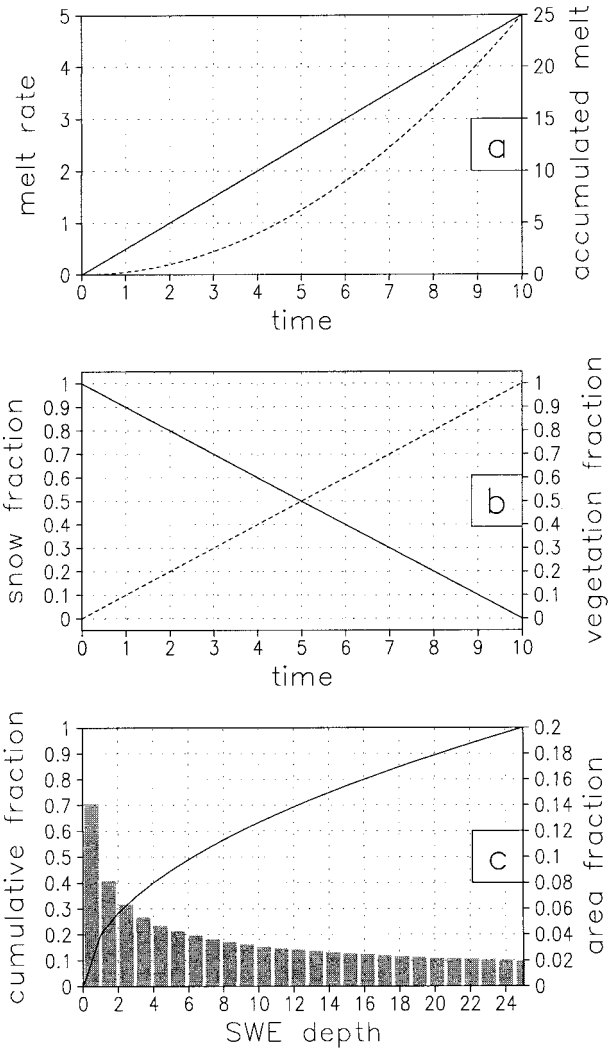

FIG. 8. Analytical examples of (a) snowmelt rate (solid line, left axis) and accumulated snowmelt (dashed line, right axis), (b) snow cover depletion (solid line, left axis) and vegetation exposure (dashed line, right axis), and (c) cumulative (solid line, left axis) and discrete (shaded bars, right axis) SWE distribution.

$$V_{\text{frac}}(t^*) = \frac{t^*}{10} \qquad (0 \le t^* \le 10) \tag{16}$$

(Fig. 8b), and by Eq. (9)

$$A^* = \frac{t^*}{10}. \tag{17}$$

Alternatively, Eq. (17) can be obtained from Eq. (15) by application of Eq. (4) and Eq. (13). Equation (14) can be used to obtain a depth–time relationship by application of Eq. (12),

$$\zeta_{\max} = \frac{t^{*2}}{4}. \tag{18}$$

Alternatively, Eq. (18) can be obtained by using Eq. (14) in Eq. (3) to get

$$M_{\text{acc}}(t^*) = \frac{t^{*2}}{4} \qquad (0 \le t^* \le 10) \tag{19}$$

(Fig. 8a), and then applying Eq. (19) in Eq. (2). Solving Eqs. (17) and (18) for t^*, and setting the resulting equations equal to each other, yields

$$A^* = \frac{\zeta_{\max}^{1/2}}{5} \tag{20}$$

(Fig. 8c). Taking the derivative of Eq. (20) yields

$$dA = \frac{\zeta_{\max}^{-1/2}}{10} d\zeta, \tag{21}$$

and allows plotting of the distribution (Fig. 8c) in a format consistent with that in Fig. 3b. Thus, the snow distribution has been generated from knowledge of the melt rate and the snow cover depletion.

In a similar manner, the snow cover depletion can be generated from knowledge of the melt rate [Eq. (14)] and the snow distribution [Eq. (20)]. As before, Eq. (14) can be used in Eq. (12) to determine $\zeta_{\max}(t^*)$ [Eq. (18)], which is then substituted into Eq. (20) to yield $A^*(t^*)$ [Eq. (17)]. The area A^* now can be used to compute the snow cover depletion through application of Eqs. (9) and (6). Last, by following a similar procedure, the snow cover depletion can be used in conjunction with the snow distribution to reconstruct the melt rate.

3. Discussion

The weather, climate, hydrologic, and ecologic research communities are striving to address the impacts and feedbacks within the completely coupled and fully interacting surface–atmosphere system, and these issues are being addressed at local, regional, and global scales. Part of this effort requires an accounting for the role that snow cover plays in the interactions between land-related features and the atmosphere. Numerous studies have shown that snow cover interacts with the earth–atmosphere system at a wide range of spatial scales, ranging from local (a few kilometers or less) (e.g., Billings 1969; Baker et al. 1992; Liston 1995; Marsh and Pomeroy 1996; Cline 1997; Neumann and Marsh 1998) and regional (tens–hundreds of kilometers) (e.g., Wagner 1973; Dewey 1977; Namias 1985; Segal et al. 1991a), to global (hundreds–thousands of kilometers) (e.g., Yeh et al. 1983; Barnett et al. 1989; Leathers and Robinson 1993; Walland and Simmonds 1997). Fortunately, under the assumption that the melt rates are uniform over the subdomain (e.g., grid cell) under consideration, the interrelationships highlighted by Eqs. (2)–(13) hold at all of these scales. In the following presentation, methods will be introduced that apply the interrelationships of Eqs. (2)–(13) to assist in solving some example problems of atmospheric, hydrologic, and ecologic interest.

a. Atmospheric examples

One way to include the three primary characteristics of seasonal snow evolution is to use subgrid models to distribute and to evolve the snow cover within each larger-scale grid cell (e.g., Liston et al. 1999a). Such a scheme likely would include such factors as snow redistribution by wind transport processes (e.g., Liston and Sturm 1998), and the subgrid precipitation distribution [using statistical approaches (e.g., Hevesi et al. 1992a,b; Daly et al. 1994; Thornton et al. 1997) or physically based approaches (e.g., Choularton and Perry 1986; Barros and Lettenmaier 1993a,b; Leung and Ghan 1995)]. Including these factors at subgrid scales in an atmospheric model, for example, allows the simulation of the snow distribution given in Fig. 3b for each atmospheric model grid cell. In addition, subgrid melt routines that include such factors as topographic slope and aspect relationships that affect subgrid solar radiation distribution and its influence on melt, and subgrid elevation differences that influence temperature distributions and melt rates, can be used to simulate the melt rates given in Fig. 3a. These melt rates and the snow distribution then can be combined to yield the snow cover depletion of Fig. 3c. This approach involves running a higher-resolution model over the domain of interest and does not take advantage of the interrelationships among Figs. 3a–c that were outlined in section 2.

The following example does use the section 2 interrelationships. In atmospheric modeling, a common question is how to represent the areal snow coverage within each atmospheric model grid cell. This question is important because the relative difference in albedo between a snow-covered area (say, an albedo of 0.80) and an area of exposed vegetation (say, an albedo of 0.15) leads to large differences in surface net radiation and thus to large differences in surface sensible and latent energy fluxes that interact with the atmosphere. A common solution is to define the grid cell to have 100% snow coverage if the snow depth is above some threshold value and then to define the fractional coverage to decrease linearly for depth values below that threshold (Foster et al. 1996). By making use of the interrelationships presented in section 2, such an oversimplification of the natural system is no longer required. Using historical snow distribution and areal depletion data such as those available from NOHRSC, representative snow distribution histograms for each atmospheric model grid cell can be generated. If the observed snow depth distribution for each grid cell is nondimensionalized by dividing by something like the model's mean gridcell snow depth, then the resulting distribution can be used to scale the mean snow depth produced by the atmospheric model. This scaling leads to a modeled snow distribution that matches that which is generally observed, while preserving the snow depth magnitude simulated by the atmospheric model. One reason why this approach is reasonable is that, while

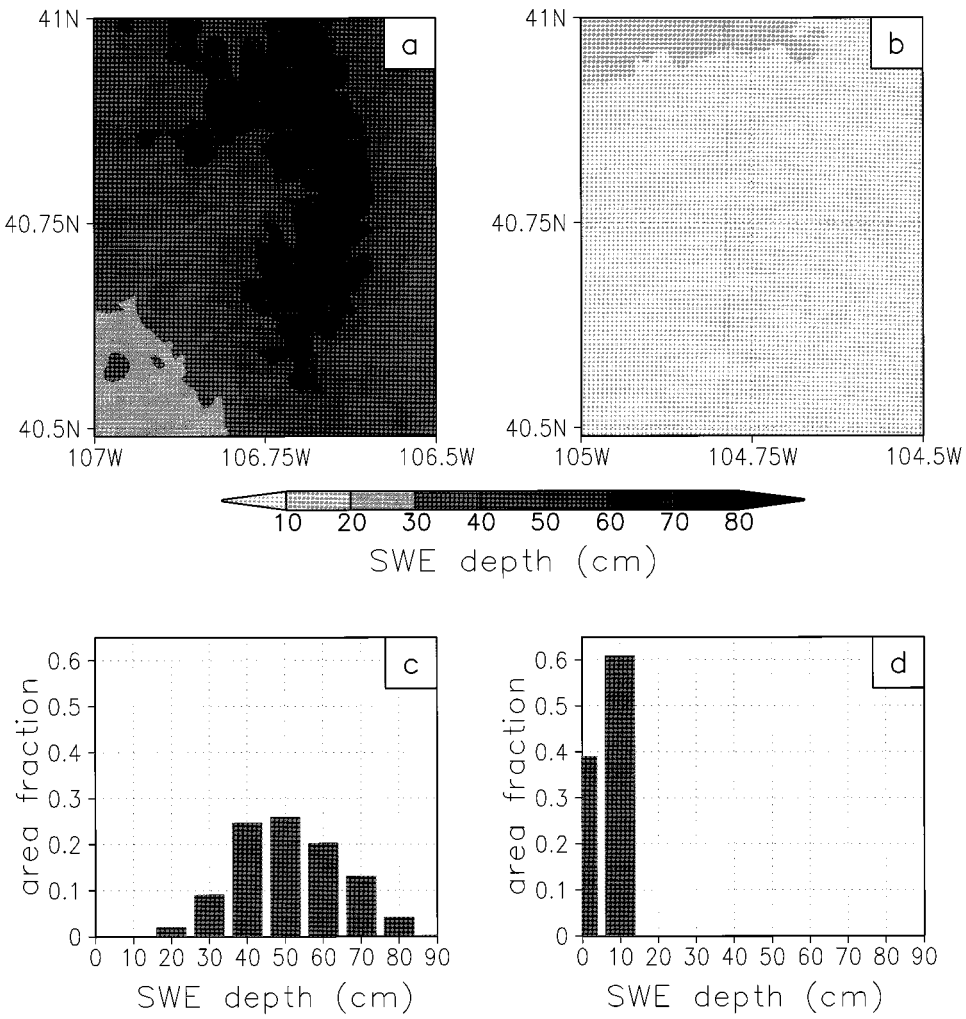

FIG. 9. NOHRSC SWE depth distributions for 0.5° lat × 0.5° long grid cells covering (a) a portion of the Colorado Rocky Mountains, and (b) the Colorado prairie for 23 Jan 1997. Also shown are the area-fraction distributions for (c) the mountain and (d) the prairie grid cells.

the actual snow depths are expected to vary from one year to the next, the *patterns* described by these distribution histograms are expected to be location specific and show little interannual variation at each location. This lack of variation happens because, for a given location, from year to year the factors that influence the snow characteristics and distribution are generally the same (Sturm et al. 1995). These factors are typically climate related, and include such things as prevailing storm winds that typically are of a similar magnitude and come from a similar direction, precipitation–topography relationships that are similar, and air temperatures that are similar. It also is recognized that these similarities do not always hold, and that regions near climatic boundaries may show considerable differences from one year to the next because of variations in large- and regional-scale atmospheric circulation patterns. These interannual changes can be the result of general climatic variability or the result of specific climate-related events such as El Niño or La Niña.

As a visual example of these ideas, consider Figs. 9a–d, which contain the 23 January 1997 NOHRSC snow distributions for 0.5° latitude by 0.5° longitude grid cells that cover the northern Colorado Rocky Mountains and the Colorado prairie. These patterns are the snow distribution patterns we would expect intuitively for these two different regions and they likely will be similar from one year to the next. Thus, such datasets can be used to define the general distribution patterns for each grid cell within the atmospheric model domain. The total snow within each grid cell, as defined by the atmospheric model, would then be forced to conform to this distribution pattern, and any melt simulated by the model then could include the subsequent knowledge of the fractional snow-covered area. Further insight into the general behavior of different snow-related land-

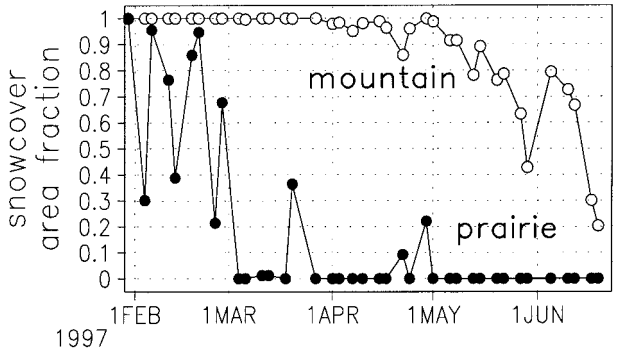

FIG. 10. Evolution of snow-covered area for the mountainous domain of Fig. 9a and for the prairie domain of Fig. 9b. These curves were generated using NOHRSC snow distribution observations, where the markers indicate observation dates.

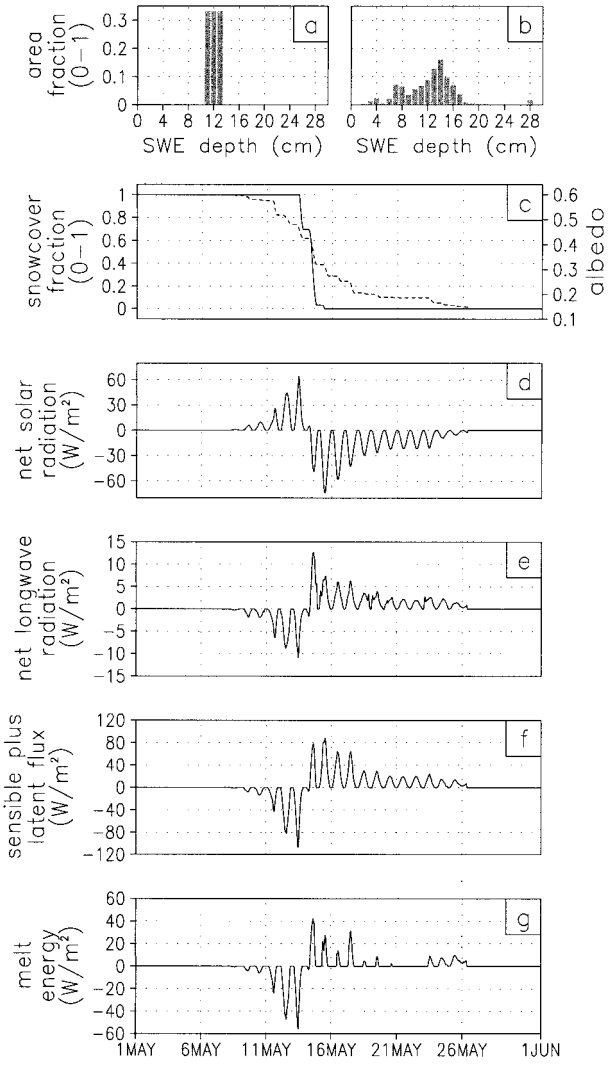

FIG. 11. (a) Gridcell SWE distributions using a typical GCM approach. (b) An observed SWE distribution. (c) Snow cover depletion (left axis) during melt for the GCM-type snow distribution (solid line) and the observed snow distribution (dashed line). Also included in (c) is the gridcell-averaged albedo evolution (right axis), where the melting-snow and vegetation albedos were defined to be 0.6 and 0.15, respectively. Panels (d)–(g) display the difference between the observed snow distribution (b) and the GCM-type snow distribution (a), that is, (b)–(a), for the melt-period energy flux components. Fluxes toward the surface are defined to be positive.

scapes and climates can be gained by looking at the January–June areal snow cover depletion curves (Fig. 10), generated from NOHRSC snow distributions, for the two domains given in Fig. 9. The snow-covered area for the mountain domain is constant throughout the winter and decreases gradually during the spring. During the spring months, mountain precipitation events occur that rebuild the snow-covered area during the general ablation period. In contrast, the prairie domain goes through relatively rapid accumulation and ablation events throughout the winter and spring seasons. Related to the differences in snow cover depletion is the fact that the areal snow distributions in the two regions differ dramatically (Fig. 9). The mountain region is characterized by large spatial variability in SWE depth, and the prairie snow cover largely is uniform. As a consequence, the mountain snow cover evolves much more slowly. The prairie region can be covered quickly by a thin film of snow and it also can be depleted quickly as that snow melts. A key feature illustrated by the snow cover depletion curves in Fig. 10, in contrast to the example Arctic snow cover, is that the midlatitude (Colorado) snow cover experiences numerous accumulation and melt events during the snow season. This variability can be thought of as several arctic-type winter–spring accumulation–ablation events, in which the accumulation and melt events may or may not progress to 100% snow coverage or to 100% snow depletion. These ideas currently are being implemented in the Colorado State University Regional Atmospheric Modeling System (Pielke et al. 1992; Liston et al. 1999a).

As a quantitative example of the improved realism gained in surface energy balance computations that use realistic snow distributions, consider the following example of two different snow distributions: the first is the observed SWE distribution given in Fig. 1 (6 May panel); the second distribution preserves the mean SWE depth from the first distribution but forces the SWE depth distribution to increase linearly over a range of depths equal to the mean of the first sample distribution $\pm$ 1.5 cm; this distribution yields an SWE depth range of 3 cm, or about 10–15 cm of snow. This second approach is consistent with the frequently used general circulation model (GCM) methodology of holding the gridcell snow coverage at 100% when depths are greater than some threshold value (typically 5–15 cm of snow), and decreasing the snow coverage linearly with depth below that value (Foster et al. 1996). These distributions are illustrated in Figs. 11a and 11b for the GCM distribution and the observed distribution, respectively. When these two sample snow distributions are melted off using the observed

hourly atmospheric forcing given in Fig. 2 and the surface energy balance model (Eq. 1), they yield the snow cover depletion of Fig. 11c. Also included in Fig. 11c is the evolution of area-averaged albedo; for these simulations the melting-snow albedo and the exposed-vegetation albedo were defined to be 0.6 and 0.15, respectively. The changes in snow cover depletion timing produce significant variations in the surface energy balance partitioning; these variations are illustrated in Figs. 11d–g, in which the differences between the realistic snow distribution (Fig. 11b) and the ''typical'' GCM distribution (Fig. 11a) are plotted. In this example, feedbacks between the surface and atmosphere have not been accounted for, so the incoming solar and longwave radiation components of the surface energy balance are the same for the two simulations. The albedo differences influence the net solar radiation (Fig. 11d) and, because the melting snow surface cannot rise above the freezing temperature, the presence of snow modifies the net longwave radiation through its influence on the outgoing surface longwave radiation (Fig. 11e). The turbulent exchange of sensible and latent heat also depends strongly upon the presence or lack of snow cover (Fig. 11f), and the existence of snow influences the partitioning of available energy into melting (Fig. 11g).

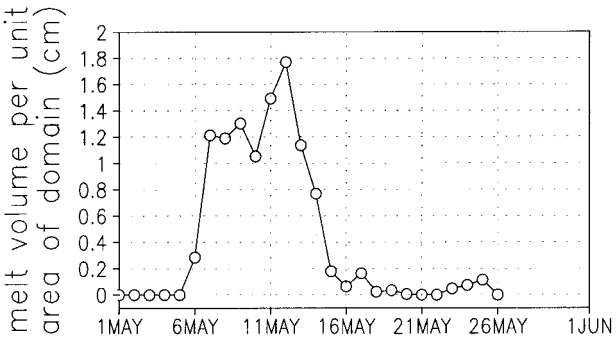

FIG. 12. Volume of meltwater produced per unit area of the domain for the SWE distribution of Fig. 3b and the melt rates of Fig. 3a.

b. Hydrologic examples

An advantage to describing the snow cover evolution following the approach outlined in section 2 and highlighted by Fig. 3 is that combining the melt and snow distribution curves allows a computation of the snowmelt volume. Numerous studies have noted that the depletion of snow-covered area is related strongly to runoff (e.g., Miller 1953; Ffolliott and Hansen 1968; Leaf 1969; U.S. Army Corps of Engineers 1971; Anderson 1973; Ferguson 1984; Buttle and McDonnell 1987), but the precise relationship is not well documented in the literature. Under the assumption of an instantaneous response (i.e., no liquid storage in the snowpack), the melt volume M_{vol} produced within a model grid cell at time t is given by

$$M_{\text{vol}}(t) = A_{\text{grid}} M_{\text{rate}}(t) S_{\text{frac}}(t)\, dt, \tag{22}$$

where A_{grid} is the gridcell area. For the example case highlighted by Fig. 3, the resulting snowmelt volume is given in Fig. 12. The expression for the total accumulated melt volume $M_{\text{acc\_vol}}$ at time t^* is

$$M_{\text{acc\_vol}}(t = t^*) = A_{\text{grid}} \int_{t=0}^{t=t^*} M_{\text{rate}}(t) S_{\text{frac}}(t)\, dt. \tag{23}$$

Depending on the specific application and the information available, Eqs. (22) and (23) can be cast in different forms using the ideas presented in Eqs. (2)–(13). For example, the $S_{\text{frac}}(t)$ term also could be represented by $[1 - A^*(t)]$ because of the relationships outlined in Eqs. (6) and (9). Such an accounting for the snowmelt volume within each model grid cell can provide the meltwater inputs to a land surface hydrology model that accounts for processes such as evaporation, transpiration, soil moisture changes, and subsequent gridcell runoffs. When this runoff is coupled to a hydrologic runoff-routing model, the resulting hydrographs can be compared to observed river and stream discharges, providing a validation tool for assessing the snow evolution simulation (e.g., Vörösmarty et al. 1989; Liston et al. 1994; Marengo et al. 1994; Miller et al. 1994).

c. Ecologic examples

As noted in the introduction, the snow distribution can have a large impact on the evolution of vegetation cover. As an example, Billings (1969) suggested that the evolution of some near-timberline forests in the Rocky Mountains were the result of interactions between the trees themselves and how they influenced the local snow distribution patterns. He hypothesized that, during the winter, snow accumulates in the lee of any trees that have started to become established. Then, during the melt of that snow cover, the most favorable moisture and light conditions for seedling establishment occur at the location of the snow cover edge in late June or early July. Areas covered by snow after this early July date are unable to establish tree seedlings because of the short snow-free ''growing season.'' These interactions lead to a striped pattern of trees and meadows that are aligned perpendicular to the prevailing winter storm winds. Billings (1969) referred to these as ''ribbon forests.'' Thus, the interrelationships among the snow distribution, snowmelt, and the depletion of snow-covered area have influenced the vegetation distribution.

These relationships among snowcover, available moisture, and growing-season length are implicit also in the interrelationships between snow distribution and vegetation patterns observed in the Arctic, where relatively deep, moderate, and shallow snow covers each are associated with specific types of vegetation (Evans et al. 1989). In another Arctic study, M. Sturm (1998, personal communication) studied the interactions and relationships between shrubs and the snow distribution

and proposed a positive feedback loop by which increased shrubs can lead to increased vegetation capture of wind-transported snow. As part of these interactions, the presence of shrubs, as opposed to lower-growing tundra, leads to increased snow depths, better thermal insulation from low winter temperatures, higher soil temperatures, and increased melt-related moisture, all of which favor shrub growth. Because of the interrelationships presented in section 2, the greater snow depth is expected to delay the snow-free date and thus shorten the growing season. Again, the interrelationships among snow distribution, melt, and areal depletion have influenced the vegetation evolution.

d. Additional considerations

The preceding discussions have largely considered a snow evolution behavior characterized by the relatively simple Arctic snow evolution system. In practice, as part of a general application of the ideas presented herein, the following issues are expected to arise. One notable difference between the Arctic and midlatitude environments is that the warmer climates typically experience numerous snow accumulation and ablation events throughout the year. This difference can be handled by forcing the accumulation to occur in the same pattern as described by the shape of the general histogram (e.g., Figs. 3b, 9c and 9d). An additional concern is that for relatively large grid cells in complex topographic regions (e.g., Fig. 9a), it is incorrect to let the melt rate be uniform over the entire grid cell (as was done in the presentation of section 2). This assumption typically is made in atmospheric models, and thus this approach is consistent with those model formulations. Factors in addition to the snow distribution that influence the snow cover depletion all relate to variables that lead to spatial variations in the melt rate. These factors include topographic slope and aspect influences on shortwave radiation reaching the surface, vegetation influences on shortwave and longwave radiation, temperature and humidity variations with elevation, and spatial distributions of wind speed. If an accounting for subgrid temperature, radiation, etc., were made, then the interrelationships outlined in section 2 would be applicable at subgrid scales to those regions of the domain where the melt rates could be assumed to be uniform.

As part of the melt-rate computations, there are expected to be feedbacks between the exposure of vegetation and the melt rate. Liston (1995) and Neumann and Marsh (1998) discussed some of these interactions that result from local advection within the atmospheric boundary layer. Additional feedbacks are expected at larger scales, where mesoscale circulations are initiated because of snow distribution variations (Segal et al. 1991a,b), but the importance of atmospheric interactions between snow-free areas and snow-covered areas still largely is unknown. Even with such feedbacks, the interrelationships presented in section 2 still hold.

The interactions among weather, climate, hydrology, and ecosystems are inherently global in scope. As such, remote sensing is expected to play a key role in monitoring and understanding global snow cover evolution. Modeling techniques that include remote sensing products are of high value, and observations of snow-covered area using remote sensing technology are becoming more frequent and of higher quality. Daily observations of snow-covered area are well matched with the general snow cover evolution and associated interactions with atmospheric and hydrologic processes, and should be used to generate snow cover depletion curves for the examples considered herein. Data obtained at frequencies less than daily still are of value but will contribute to errors resulting from accumulation and ablation events that occur at higher frequencies; an example of this contribution is the error produced in Fig. 7 for SWE depths between 5 and 7 cm.

The specific problem under consideration will determine the required spatial resolution. Currently, continental-scale snow cover and snow distribution products are available at grid increments of approximately 1 km (Carroll 1997). These products are quite adequate for regional and global atmospheric modeling programs, although it is recognized that many snow distribution–related features occur at scales much smaller than 1 km, for example, the erosion and deposition of snow around ridges, bluffs, gullies, and trees (e.g., Liston and Sturm 1998). To address such local-scale issues, finer-scale snow cover data are required. Cline et al. (1998) provided an example application of such finescale snow cover data, and discussed remote sensing methods that resolve subpixel snow cover information. Because in windy environments snow frequently accumulates in deep drifts of relatively small spatial extent, such datasets are expected to contribute strongly to the understanding of fractional snow-covered area.

4. Conclusions

In light of the role that snow cover plays in modifying weather, climate, hydrologic, and ecologic features, recent modeling efforts are working to improve their representations of seasonal snow cover. A mathematical description of the interrelationships among the end-of-winter SWE depth distribution, the melt rate, and the snow cover depletion has been presented. This description, in turn, suggests how snow cover extent data and snowmelt computations can be combined to reconstruct the subgrid, end-of-winter SWE depth distribution. In addition, improvements in the ability of remote sensing to provide snow-related products to the weather, climate, hydrologic, and ecologic communities are rapidly evolving, and the ability of remote sensing to distinguish between snow-covered and snow-free areas has been particularly successful (Cline et al. 1998). For example, the production of daily, global snow cover extent data at subkilometer spatial scales appears to be a realistic

short-term goal [e.g., the NASA snow-mapping (SNOMAP) algorithm (Hall et al. 1995), which uses data collected by the Earth Observing System (EOS) Moderate Resolution Imaging Spectroradiometer (MODIS)]. The combination of these factors represents an opportunity to improve subgrid-scale snow distribution representations in modeling efforts where snow is an important component.

The spatial distribution of snow-covered area is a key input to atmospheric and hydrologic models. In addition, during snowmelt, knowledge of the SWE depth distribution is required, because it is the variable depth distribution that largely leads to the patchy mosaic of snow and vegetation that develops as the snow melts. Consider, for example, that the areal coverage represented by Figs. 3a–c is the area of a single regional or global atmospheric model grid cell (with cell sizes ranging from a few kilometers to a few hundred kilometers). The features represented by Figs. 3a–c are strongly interrelated; the subgrid-scale exposure of vegetation influences the snowmelt rate, and applying the melt rates to the within-grid snow distribution leads to the exposure of vegetation.

The ideas presented herein suggest that knowledge of the snow distribution also is required to compute correctly the energy and moisture fluxes (net solar and longwave radiation, sensible and latent heat, and melt energy) that occur among the land, snow, and atmosphere during snowmelt periods. As an alternative, knowledge of the snow-covered area evolution can be combined with the melt-energy computations as a substitute for the snow distribution information. The availability of remote sensing products that define the snow-covered area, in conjunction with an atmospheric or hydrologic model appropriately handling the snowmelt computation, compose the tools required to simulate the fundamental subgrid-scale features of the seasonal snow cover evolution while appropriately simulating the associated energy and moisture fluxes. The development of a methodology that directly accounts for the influence of subgrid-scale snow cover variability within the context of regional and global weather, climate, hydrologic, and ecologic models is expected to improve key features of the model-simulated interactions between the land and atmosphere during the winter and spring months.

Acknowledgments. The author would like to thank Ethan Greene, Dorothy Hall, Chris Hiemstra, Roger Pielke Sr., William Reiners, and Matthew Sturm for their discussions regarding the ideas and applications that have gone into this paper. This work was supported by NOAA Grant NA67RJ0152, NASA Grant NAG5-4760 and P.O. S-10100-G, CRREL Agreement DACA89-97-2-0001, and NSF Grant OPP-9415386.

REFERENCES

Anderson, E. A., 1973: National Weather Service river forecast system—Snow accumulation and ablation model. NOAA Tech. Memo. NWS HYDRO-17, 217 pp.

Baker, D. G., D. L. Ruschy, R. H. Skaggs, and D. B. Wall, 1992: Air temperature and radiation depressions associated with a snow cover. *J. Appl. Meteor.,* **31,** 247–254.

Barnett, T. P., L. Dümenil, U. Schlese, E. Roeckner, and M. Latif, 1989: The effect of Eurasian snow cover on regional and global climate variations. *J. Atmos. Sci.,* **46,** 661–685.

Barros, A. P., and D. P. Lettenmaier, 1993a: Dynamic modeling of orographically induced precipitation. *Rev. Geophys.,* **32,** 265–284.

——, and ——, 1993b: Dynamic modeling of the spatial distribution of precipitation in remote mountainous areas. *Mon. Wea. Rev.,* **121,** 1195–1214.

Billings, W. D., 1969: Vegetational patterns near alpine timberline as affected by fire–snowdrift interactions. *Vegetatio,* **19,** 192–207.

Buttle, J. M., and J. J. McDonnell, 1987: Modelling the areal depletion of a snow cover in a forested catchment. *J. Hydrol.,* **90,** 43–60.

Carroll, T. R., 1997: Integrated observations and processing of snow cover data in the NWS hydrology program. Preprints, *First Symp. on Integrated Observing Systems,* Long Beach, CA, Amer. Meteor. Soc., 180–183.

Choularton, T. W., and S. J. Perry, 1986: A model of the orographic enhancement of snowfall by the seeder–feeder mechanism. *Quart. J. Roy. Meteor. Soc.,* **112,** 335–345.

Cline, D. W., 1997: Effect of seasonality of snow accumulation and melt on snow surface energy exchanges at a continental alpine site. *J. Appl. Meteor.,* **36,** 32–51.

——, R. C. Bales, and J. Dozier, 1998: Estimating the spatial distribution of snow in mountain basins using remote sensing and energy balance modeling. *Water Resour. Res.,* **34,** 1275–1285.

Daly, C., 1984: Snow distribution patterns in the alpine krummholz zone. *Progress Phys. Geog.,* **8,** 157–175.

——, R. P. Neilson, and D. L. Phillips, 1994: A statistical–topographic model for mapping climatological precipitation over mountainous terrain. *J. Appl. Meteor.,* **33,** 140–158.

Dewey, K. F., 1977: Daily maximum and minimum temperature forecasts and the influence of snow cover. *Mon. Wea. Rev.,* **105,** 1594–1597.

Douville, H., J.-F. Royer, and J.-F. Mahfouf, 1995: A new snow parameterization for the Météo-France climate model. Part I: Validation in stand-alone experiments. *Climate Dyn.,* **12,** 21–35.

Dunne, T., and L. B. Leopold, 1978: *Water in Environmental Planning.* W. H. Freeman and Company, 818 pp.

Essery, R. L. H., 1997: Modelling fluxes of momentum, sensible heat and latent heat over heterogeneous snow cover. *Quart. J. Roy. Meteor. Soc.,* **123,** 1867–1883.

Evans, B. M., D. A. Walker, C. S. Benson, E. A. Nordstrand, and G. W. Petersen, 1989: Spatial interrelationships between terrain, snow distribution, and vegetation patterns at an arctic foothills site in Alaska. *Holarctic Ecol.,* **12,** 270–278.

Ferguson, R. I., 1984: Magnitude and modelling of snowmelt runoff in the Cairngorm Mountains, Scotland. *Hydrol. Sci. J.,* **29,** 49–62.

Ffolliott, P. F., and E. A. Hanson, 1968: Observations of snowpack accumulation melt and runoff on a small Arizona watershed. Res. Note RM-124, U.S. Forest Service, 7 pp.

Foster, J., and Coauthors, 1996: Snow cover and snow mass intercomparisons of general circulation models and remotely sensed datasets. *J. Climate,* **9,** 409–426.

Griggs, R. F., 1938: Timberlines in the northern Rocky Mountains. *Ecology,* **19,** 548–564.

Hall, D. K., 1988: Assessment of polar climate change using satellite technology. *Rev. Geophys.,* **26,** 26–39.

——, G. A. Riggs, and V. V. Salomonson, 1995: Development of methods for mapping global snow cover using moderate resolution imaging spectroradiometer data. *Remote Sens. Environ.,* **54,** 127–140.

Hevesi, J. A., A. L. Flint, and J. D. Istok, 1992a: Precipitation estimation in mountainous terrain using multivariate geostatistics. Part II: Isohyetal maps. *J. Appl. Meteor.,* **31,** 667–688.

——, J. D. Istok, and A. L. Flint, 1992b: Precipitation estimation in mountainous terrain using multivariate geostatistics. Part I: Structural analysis. *J. Appl. Meteor.,* **31,** 661–676.

Kane, D. L., L. D. Hinzman, C. S. Benson, and G. E. Liston, 1991: Snow hydrology of a headwater Arctic basin. 1. Physical measurements and process studies. *Water Resour. Res.,* **27,** 199–1109.

König, M., and M. Sturm, 1998: Mapping snow distribution in the Alaskan Arctic using air photos and topographic relationships. *Water Resour. Res.,* **34,** 3471–3483.

Leaf, C. F., 1969: Aerial photographs for operational streamflow forecasting in the Colorado Rockies. *Proc. 37th Annual Meeting Western Snow Conf.,* Salt Lake City, UT, 19–28.

Leathers, D. J., and D. A. Robinson, 1993: The association between extremes in North American snow cover extent and United States temperatures. *J. Climate,* **6,** 1345–1355.

Leung, R. L., and S. J. Ghan, 1995: A subgrid parameterization of orographic precipitation. *Theor. Appl. Climatol.,* **52,** 95–118.

Liston, G. E., 1986: Seasonal snowcover of the foothills region of Alaska's Arctic slope: A survey of properties and processes. M.S. thesis, University of Alaska, Fairbanks, 123 pp.

——, 1995: Local advection of momentum, heat, and moisture during the melt of patchy snow covers. *J. Appl. Meteor.,* **34,** 1705–1715.

——, and D. K. Hall, 1995: An energy balance model of lake ice evolution. *J. Glaciol.,* **41,** 373–382.

——, and M. Sturm, 1998: A snow-transport model for complex terrain. *J. Glaciol.,* **44,** 498–516.

——, Y. C. Sud, and E. F. Wood, 1994: Evaluating GCM land surface hydrology parameterizations by computing river discharges using a runoff routing model: Application to the Mississippi Basin. *J. Appl. Meteor.,* **33,** 394–405.

——, R. A. Pielke Sr., and E. M. Greene, 1999a: Improving first-order snow-related deficiencies in a regional climate model. *J. Geophys. Res.,* in press.

——, J.-G. Winther, O. Bruland, H. Elvehøy, and K. Sand, 1999b: Below-surface ice-melt on the coastal Antarctic ice sheet. *J. Glaciol.,* **45,** 273–285.

Loth, B., and H.-F. Graf, 1998a: Modeling the snow cover in climate studies. 1. Long-term integrations under different climatic conditions using a multilayered snow-cover model. *J. Geophys. Res.,* **103** (10), 11 313–11 327.

——, and ——, 1998b: Modeling the snow cover in climate studies. 2. The sensitivity to internal snow parameters and interface processes. *J. Geophys. Res.,* **103** (10), 11 329–11 340.

Lynch-Stieglitz, M., 1994: The development and validation of a simple snow model for the GISS GCM. *J. Climate,* **7,** 1842–1855.

Male, D. H., and D. M. Gray, 1981: Snowcover ablation and runoff. *Handbook of Snow, Principles, Processes, Management and Use,* D. M. Gray and D. H. Male, Eds., Pergamon Press, 360–436.

Marengo, J. A., J. R. Miller, G. L. Russell, C. E. Rosenzweig, and F. Abramopoulos, 1994: Calculations of river-runoff in the GISS GCM: Impact of a new land-surface parameterization and runoff routing model on the hydrology of the Amazon River. *Climate Dyn.,* **10,** 349–361.

Marsh, P., and J. W. Pomeroy, 1996: Meltwater fluxes at an Arctic forest–tundra site. *Hydrol. Processes,* **10,** 1383–1400.

Marshall, S., and R. J. Oglesby, 1994: An improved snow hydrology for GCMs. Part 1: Snow cover fraction, albedo, grain size, and age. *Climate Dyn.,* **10,** 21–37.

——, J. O. Roads, and G. Glatzmaier, 1994: Snow hydrology in a general circulation model. *J. Climate,* **7,** 1251–1269.

Martinec, J., and A. Rango, 1981: Areal distribution of snow water equivalent evaluated by snow cover monitoring. *Water Resour. Res.,* **17,** 1480–1488.

——, and ——, 1986: Parameter values for snowmelt runoff modeling. *J. Hydrol.,* **84,** 197–219.

——, and ——, 1987: Interpretation and utilization of areal snowcover data from satellites. *Ann. Glaciol.,* **9,** 166–169.

Miller, D. M., 1953: Snow cover depletion and runoff. Snow Investigation Research Note No. 16, U.S. Army Corps of Engineers, Pacific Division, Portland, OR, 16 pp.

Miller, J. R., G. L. Russell, and G. Caliri, 1994: Continental-scale river flow in climate models. *J. Climate,* **7,** 914–928.

Namias, J., 1985: Some empirical evidence for the influence of snow cover on temperature and precipitation. *Mon. Wea. Rev.,* **113,** 1542–1553.

Neumann, N., and P. Marsh, 1998: Local advection of sensible heat in the snowmelt landscape of Arctic tundra. *Hydrol. Processes,* **12,** 1547–1560.

Pielke, R. A., and Coauthors, 1992: A comprehensive meteorological modeling system—RAMS. *Meteor. Atmos. Phys.,* **49,** 69–91.

Rango, A., and J. Martinec, 1979: Application of a snowmelt-runoff model using Landsat data. *Nord. Hydrol.,* **10,** 225–238.

——, 1993: II. Snow hydrology processes and remote sensing. *Hydrol. Processes,* **7,** 121–138.

Segal, M., J. H. Cramer, R. A. Pielke, J. R. Garratt, and P. Hildebrand, 1991a: Observational evaluation of the snow breeze. *Mon. Wea. Rev.,* **119,** 412–424.

——, J. R. Garratt, R. A. Pielke, and Z. Ye, 1991b: Scaling and numerical model evaluation of snow-cover effects on the generation and modification of daytime mesoscale circulations. *J. Atmos. Sci.,* **48,** 1024–1042.

Shook, K., D. M. Gray, and J. W. Pomeroy, 1993: Temporal variation in snowcover area during melt in prairie and alpine environments. *Nord. Hydrol.,* **24,** 183–198.

Slater, A. G., A. J. Pitman, and C. E. Desborough, 1998: The validation of a snow parameterization designed for use in general circulation models. *Int. J. Climatol.,* **18,** 595–617.

Sturm, M., J. Holmgren, and G. E. Liston, 1995: A seasonal snow cover classification system for local to global applications. *J. Climate,* **8,** 1261–1283.

Thornton, P. E., S. W. Running, and M. A. White, 1997: Generating surfaces of daily meteorological variables over large regions of complex terrain. *J. Hydrol.,* **190,** 214–251.

U.S. Army Corps of Engineers, 1956: *Snow Hydrology, Summary Report of the Snow Investigations.* U.S. Government Printing Office, 433 pp.

——, 1971: *Runoff Evaluation and Streamflow Simulation by Computer. Part II.* U.S. Army Corps Eng., 117 pp.

Verseghy, D. L., 1991: CLASS—A Canadian land surface scheme for GCMs. I: Soil model. *Int. J. Climatol.,* **11,** 111–133.

Vörösmarty, C. J., B. Moore III, A. L. Grace, M. P. Gildea, J. M. Melillo, B. J. Peterson, E. B. Rastetter, and P. A. Steudler, 1989: Continental scale models of water balance and fluvial transport: an application to South America. *Global Biogeochem. Cycles,* **3,** 241–268.

Wagner, A. J., 1973: The influence of average snow depth on monthly mean temperature anomaly. *Mon. Wea. Rev.,* **101,** 624–626.

Walker, D. A., J. C. Halfpenny, M. D. Walker, and C. A. Wessman, 1993: Long-term studies of snow–vegetation interactions. *BioScience,* **43,** 287–301.

Walland, D. J., and I. Simmonds, 1996: Sub-grid-scale topography and the simulation of Northern Hemisphere snow cover. *Int. J. Climatol.,* **16,** 961–982.

——, and ——, 1997: Modelled atmospheric response to changes in Northern Hemisphere snow cover. *Climate Dyn.,* **13,** 25–34.

WMO, 1986: Intercomparison of models of snowmelt runoff. World Meteorological Organization, Operational Hydrol. Rep. 23, WMO 646.

Wooldridge, G. L., R. C. Musselman, R. A. Sommerfeld, D. G. Fox, and B. H. Connell, 1996: Mean wind patterns and snow depths in an alpine-subalpine ecosystem as measured by damage to coniferous trees. *J. Appl. Ecol.,* **33,** 100–108.

Yang, Z.-L., R. E. Dickinson, A. Robock, and K. Y. Vinnikov, 1997: Validation of the snow submodel of the biosphere–atmosphere transfer scheme with Russian snow cover and meteorological observational data. *J. Climate,* **10,** 353–373.

Yeh, T.-C., R. T. Wetherald, and S. Manabe, 1983: A model study of the short-term climatic and hydrologic effects of sudden snow cover removal. *Mon. Wea. Rev.,* **111,** 1013–1024.